Biogeosciences, 22, 455–472, 2025
https://doi.org/10.5194/bg-22-455-2025

Biogeosciences Open Access EGU

How long does carbon stay in a near-pristine central Amazon forest? An empirical estimate with radiocarbon

Ingrid Chanca[1,2,a,★], **Ingeborg Levin**[3,★,†], **Susan Trumbore**[1], **Kita Macario**[2,4,5], **Jost Lavric**[1,b], **Carlos Alberto Quesada**[6], **Alessandro Carioca de Araújo**[7], **Cléo Quaresma Dias Júnior**[8], **Hella van Asperen**[1], **Samuel Hammer**[3], **and Carlos A. Sierra**[1]

[1]Department of Biogeochemical Processes, Max Planck Institute for Biogeochemistry, Jena, Germany
[2]Laboratório de Radiocarbono, Instituto de Física, Universidade Federal Fluminense, Niterói, Brazil
[3]Institute of Environmental Physics, Heidelberg University, Heidelberg, Germany
[4]Graduate Program in Geosciences (Geochemistry), Universidade Federal Fluminense, Niterói, Brazil
[5]Graduate Program in Physics, Instituto de Física, Universidade Federal Fluminense, Niterói, Brazil
[6]Coordination of Environmental Dynamics, Instituto Nacional de Pesquisas da Amazônia (INPA), Manaus, Brazil
[7]Empresa Brasileira de Pesquisa Agropecuária (EMBRAPA) Amazônia Oriental, Belém, Brazil
[8]Instituto Federal de Educação, Ciência e Tecnologia do Pará, Belém, Brazil
[a]Laboratoire des Sciences du Climat et de l'Environnement, LSCE/IPSL, CEA-CNRS-UVSQ, Université Paris-Saclay, Gif-sur-Yvette, France
[b]Environmental Division, Acoem GmbH, Hallbergmoos, Germany
★These authors contributed equally to this work.
†deceased, 10 February 2024

Correspondence: Ingrid Chanca (ichanca@bgc-jena.mpg.de)

Received: 24 March 2024 – Discussion started: 19 April 2024
Revised: 18 August 2024 – Accepted: 21 October 2024 – Published: 28 January 2025

Abstract. Amazon forests play a significant role in the global C cycle by assimilating large amounts of CO_2 through photosynthesis and by storing C largely as biomass and soil organic matter. To evaluate the net budget of C in the Amazon, we must also consider the amplitude and timing of losses of C back to the atmosphere through respiration and biomass burning. One useful timescale metric that integrates such information in terrestrial ecosystems is the transit time of C, defined as the time elapsed between C entering and leaving the ecosystem; the transit time is equivalent to the age of C exiting the ecosystem, which occurs mostly through respiration. We estimated the mean transit time of C for a central Amazon forest based on the C age during ecosystem respiration (ER), taking advantage of the large variations in CO_2 in the atmosphere below the forest canopy to estimate the radiocarbon signature of mean ER ($\Delta^{14}C_{ER}$) using Keeling and Miller–Tans mixing models. We collected air samples to evaluate changes in the isotopic signature of the main ER sources by estimating the $\delta^{13}C_{ER}$. We collected air samples in vertical profiles in October 2019 and December 2021 at the Amazon Tall Tower Observatory (ATTO) in the central Amazon. Air samples were collected in a diel cycle from two heights below the canopy (4 and 24 m above ground level (a.g.l.)). Afternoon above-canopy samples (79 and 321 m a.g.l.) were collected as the background. For the campaign of October 2019, the mean $\Delta^{14}C_{ER}$ ranged from 24 ‰ to 41 ‰ with both Keeling and Miller–Tans methods. In December 2021, mean $\Delta^{14}C_{ER}$ ranged from 53 ‰ to 102 ‰. The $\delta^{13}C_{ER}$ showed a smaller variation, being -27.8 ± 0.3 ‰ in October 2019 and -29.0 ± 0.5 ‰ in December 2021. The $\Delta^{14}C_{ER}$ estimates were compared with the record of atmospheric radiocarbon from the bomb period, providing estimates of mean transit time of 6 ± 2 years for 2019 and 18 ± 4 years for 2021. In contrast to steady-state carbon balance models that predict constant mean transit times, these results suggest an important level of variation in mean transit times. We discuss these results in the context of previous model-based estimates of mean transit time for

tropical forests and the Amazon region. In addition, we discuss previous studies that indicate that approximately 70 % of assimilated carbon is respired as autotrophic respiration in the central Amazon. Our results suggest that newly fixed carbon in this terra firme tropical forest is respired within 1 to 2 decades, implying that only a fraction of assimilated C can act as a sink for decades or longer.

1 Introduction

Tropical forests play a relevant role in the global carbon (C) cycle for two main reasons: (i) due to their high assimilation rate of carbon dioxide (CO_2) through photosynthesis (gross primary production, GPP, at ecosystem level; Beer et al., 2010; Jung et al., 2020) and (ii) due to their high storage of C in vegetation and soils, representing up to a quarter of the total C mass in terrestrial ecosystems (Carvalhais et al., 2014; Malhi et al., 2011).

In particular, the Amazon rainforest, as the largest continuous rainforest in the world, plays an important role in the global C cycle, taking up significant amounts of CO_2 from the atmosphere (Stephens et al., 2007; Malhi et al., 2015; Phillips and Brienen, 2017; Baker and Spracklen, 2019; Botía et al., 2022) and storing this carbon in terrestrial ecosystems for times that can range from hours to centuries (Sedjo and Sohngen, 2012; Sierra et al., 2021a).

Although the rates of C uptake in Amazon forests are among the largest in terrestrial ecosystems (Malhi et al., 1999), C losses through respiration are also very high, and autotrophic respiration is estimated in around two-thirds of assimilated C in the central Amazon, compensating for most of the C uptake (Chambers et al., 2004, 2013; Sierra et al., 2007; Malhi et al., 2011). Additionally, several studies have found high variability in the magnitude and direction of C fluxes in the Amazon region because of anthropogenic disturbances (e.g., fires and deforestation) and extreme drought events (e.g., associated with El Niño) (Brienen et al., 2015; Phillips and Brienen, 2017; Hubau et al., 2020; Gatti et al., 2021). Therefore, to better understand the overall carbon balance of the Amazon forests, it is important to know not only the amount of carbon uptake but also for *how long* C is retained within these ecosystems (Muñoz et al., 2023).

A key diagnostic metric for characterizing timescales of C cycling in ecosystems is the transit time of C, which can be defined as the age of C during ecosystem respiration (Rasmussen et al., 2016; Sierra et al., 2017; Lu et al., 2018). The total respiration flux of an ecosystem is composed of C that spends different amounts of time stored in different ecosystem compartments (Trumbore, 2006), and it captures the metabolic activity of both autotrophic and heterotrophic organisms. Therefore, the age of C in ecosystem respiration, i.e., the transit time of C through the ecosystem, serves as a key diagnostic metric to characterize how long, on average, a C atom is stored in ecosystems before it is respired back to the atmosphere as CO_2.

Radiocarbon (^{14}C) can be used as a tracer of C dynamics in ecosystems and to track how C moves across different ecosystem C pools. Measurements of radiocarbon in respiration can also be used to quantify the transit time of C through ecosystems (Trumbore and De Camargo, 2009). Radiocarbon is produced naturally in the upper atmosphere by the interaction of thermal neutrons from cosmic rays with ^{14}N in the atmosphere. Additionally, nuclear weapon tests in the atmosphere during the late 1950s and early 1960s produced a large number of thermal neutrons that led to the production of excess ^{14}C. After natural and anthropogenic production, ^{14}C is oxidized to CO_2 and is incorporated into the global carbon cycle. After the Limited Test Ban Treaty in 1963, the concentration of $^{14}CO_2$ in the atmosphere started to decline due to its incorporation into the biosphere and surface ocean (Levin et al., 2022). Atmospheric CO_2 containing ^{14}C that has changed over time since the 1960s is assimilated by terrestrial ecosystems in the same manner as natural isotopes of C. For instance, C in freshly fixed plant metabolites (e.g., leaf sugars) will have the same ratio of ^{14}C content as the atmosphere at the time they are assimilated. Yet, ^{14}C respired from organic matter decomposition would reflect the age of C used to grow plant tissue, as well as the time it takes for decomposition to occur, leading to C ages of respiration from organic matter that are generally higher than 1 year. CO_2 respired by fast-cycling pools (e.g., canopy leaves) should have a ^{14}C isotopic signature close to the contemporaneous atmospheric ^{14}C signal. Thus, the age of C in ecosystem respiration is a mix of ages of C respired from different compartments with distinct isotopic signatures and integrates the timescales of different processes such as production, allocation, and decomposition (Trumbore and De Camargo, 2009; Chanca et al., 2022).

An estimate of the whole ecosystem's respiration ^{14}C isotopic ratio can be obtained from the covariation of ^{14}C with CO_2 concentration in the air using end-member mixing analysis methods such as the Keeling plot (Keeling, 1958, 1961) or the Miller–Tans plot (Miller and Tans, 2003) methods. Traditionally, Keeling plots have been applied to terrestrial ecosystems to characterize the stable C isotopic signatures of the main sources of ecosystem respiration that have different $\delta^{13}C$ values, i.e., the deviation in parts per thousand of sample $^{13}C/^{12}C$ in comparison to a standard material (Pataki et al., 2003), but the method can also be used to obtain the radiocarbon signature of ecosystem respiration (Phillips et al., 2015). A comparison between the mean ^{14}C isotopic signature of the whole ecosystem's respiration and the time history of the ^{14}C isotopic signature in atmospheric CO_2 provides an estimate of the mean transit time for C, i.e., the time C takes to move through the whole ecosystem, from photosynthesis to respiration.

We used isotopic mixing models of radiocarbon in atmospheric CO_2 below and above the canopy level to address two questions:

i. What is the mean transit time of C for an Amazon terra firme forest as estimated with Keeling and Miller–Tans methods using $^{14}CO_2$?

ii. How does this empirical estimate compare with other model-based estimates of mean transit time for tropical forests?

To address these questions, we first provide a brief introduction to end-member mixing analysis as applied for radiocarbon measurements in CO_2, describing the sampling sites and statistical methods. We then report our estimates of mean transit times and discuss the results in the context of previous model-based estimates of mean transit time for tropical forests and the Amazon region.

2 Materials and methods

2.1 Study site

Atmospheric air samples below and above the canopy level were collected at an 80 m tall walk-up tower (coordinates (WGS 84): 02°08.6470′ S, 58°59.9920′ W) located at the Amazon Tall Tower Observatory (ATTO) site in the Uatumã Sustainable Development Reserve in the central Amazon. The ATTO site is located ca. 150 km NE of the city of Manaus. In addition, the site includes two other towers: the ATTO tall tower (02°08.7520′ S, 59°00.3350′ W; 325 m tall) and a triangular mast (02°08.6020′ S, 59°00.0330′ W; 81 m tall) (Andreae et al., 2015). Meteorological conditions are measured continuously at the 80 m walk-up tower.

The three towers are located on a plateau area, with vegetation characterized as old-growth closed-canopy terra firme (non-flooded) forest. Around the towers, the canopy rises to approximately 35 m, with emergent trees reaching 45 m above ground level (a.g.l.). Areas surrounding the tower include a network of plateaus and valleys connected by relatively steep slopes with a maximum relief height of ca. 100 m, with the base of the tall tower being located at an elevation of 120 m above sea level (a.s.l.) (Andreae et al., 2015).

The mean annual precipitation measured locally between the years 2012 and 2019 was 1934.1 mm yr^{-1} (Botía et al., 2022). Mean air temperatures do not vary strongly in the central Amazon, including at the ATTO site. However, temperature maxima at the canopy level may vary between seasons. During the dry season (August–November), the daytime temperature maxima at the canopy top are slightly above 30 °C. During the wet season (February–May), the daytime temperature maxima are around 28 °C. In both seasons, the temperature minima are around 22 °C (Andreae et al., 2015).

2.2 Sampling

Forest air samples were collected from two heights within the canopy, at 4 and 24 m a.g.l., during two campaigns conducted during the dry season and during the transition from the dry to the wet season. The first campaign took place in October 2019, and the second campaign took place in December 2021. A few samples were collected from the top level of the 80 m walk-up tower (79 m a.g.l.) to be used as a reference of the above-canopy air for the Miller–Tans plots, which consist of an approach where the values ($\Delta^{14}C$–CO_2, CO_2 concentrations) observed within the canopy are plotted after subtraction of the values observed in the tropospheric background (Miller and Tans, 2003). The canopy level at the study plot is around 35 m high, making the 79 m level reasonably appropriate as a background (Pataki et al., 2003). At the ATTO tall tower, since September 2021, air samples have been collected into flasks from 321 m a.g.l. Additionally, since February 2019, 1-month-integrated samples have been collected by means of the absorption of CO_2 in NaOH solution for radiocarbon analysis at 321 m through the method detailed by Levin et al. (1980).

Air from the different heights was collected through Synflex® metal–plastic composite tubings of 1/4″ o.d. connected at heights of 4, 24, and 79 m a.g.l. at the 80 m walk-up tower and 321 m a.g.l. at the ATTO tall tower. The air flowing from the tubing inlets was transferred to glass flasks of 3 L volume. The flasks contain valves of PCTFE (polychlorotrifluoroethylene) seals and are the standard flasks of ICOS class-1 stations (Levin et al., 2020). Before shipment and sampling, flasks were conditioned (i.e., evacuated, baked, and filled with dry air) at the ICOS Central Analytical Laboratory.

At the 80 m walk-up tower, air samples were collected with a portable flask sampler, which is a compressor module that comprises a membrane pump and compressor, and gauges for monitoring the flow of air and the pressure inside the flasks (Heimann et al., 2022). The aim is to pump air from the desired height into the flask while simultaneously compressing the air to keep a final absolute pressure of about 1.6 bar inside the flask. Additionally, a drying agent can be attached to the system; the drying agent is particularly relevant when one is interested in the $\delta^{18}O$–CO_2 (Steur et al., 2023), which was not the case here. Nevertheless, for the campaign of 2021, when the air relative humidity was high (dry-to-wet season), we decided to use anhydrous magnesium perchlorate inside a cartridge before the flask to trap the water vapor from the air and to avoid interferences in the airflow and eventual damage to the sampler due to water condensation on pieces of the equipment. Each sample was flushed for 15 min at a flow rate of ca. 2 L min^{-1}. Additional details on the standard flask sampling protocol at the Max Planck Institute for Biogeochemistry (MPI-BGC), as well as the flask sampling instructions for the portable sampler, can be found in Heimann et al. (2022).

At the ATTO tall tower, air samples were collected with an automated sampler from the ICOS network (Levin et al., 2020) from an inlet at 321 m a.g.l. once per week between 13:00 and 14:00 local time (LT, UTC-0400) at a flow of $1/t$, which guarantees that the sample represents a real 1 h mean air collection. During collection, the 3 L flasks are filled with samples of local air at about 1.6 bar absolute pressure.

Our reference background for CO_2 concentrations in 2019 consisted of flask samples taken at 79 m a.g.l. during the afternoon (13:29 and 17:09 LT). The CO_2 concentration of a sample collected on 16 December 2021 was used as the CO_2 background reference for the sub-canopy samples collected in December 2021. Background $\Delta^{14}C$–CO_2 in October 2019 was based on a 1-month-integrated sample collected between 9 September 2019 and 15 October 2019. For the background $\Delta^{14}C$–CO_2 in December 2021, two samples, collected during 24 November–19 December 2021 and 19 December 2021–26 January 2022, were averaged.

In 2019, samples of air below the canopy were collected following a 24 h cycle with sampling times of roughly every 2 h between 5 and 6 October, totaling 20 sub-canopy samples. Including the samples collected at 79 m, a total of 24 samples were collected in October 2019. On 19 and 20 December 2021, samples were collected in intervals of 3–4 h during the day and intervals of up to 8 h during the night, adding up to 12 samples. Flasks sampled between local sunrise (05:45 LT) and local sunset (18:00 LT) are considered to constitute the daytime; otherwise, they are considered to constitute the nighttime. During laboratory analyses, some samples were disregarded for being inconsistent with ambient air samples (e.g., SF_6 mole fraction equal to the one of the dry air used to fill the flasks for transport); additionally, some other flasks got broken, and so the final data comprise 18 samples for October 2019 and 10 samples for December 2021.

2.3 Analytical methods and data analyses

CO_2 concentrations and C isotope ratios ($\delta^{13}C$–CO_2 and $\Delta^{14}C$–CO_2) from flask samples were measured in the laboratories (GasLab, IsoLab, and ^{14}C-Analytik) of MPI-BGC in Jena, Germany, except for the $\Delta^{14}C$–CO_2 of samples collected in October 2019, whose values were determined by the Integrated Carbon Observation System–Central Radiocarbon Laboratory (ICOS-CRL) facility in Heidelberg University, Germany, in collaboration with the Curt-Engelhorn-Zentrum Archäometrie (CEZA) AMS facility in Mannheim, Germany.

The CO_2 concentrations inside the flasks were measured in the GasLab at MPI-BGC with an Agilent 6890 gas chromatograph equipped with an electron capture detector (ECD) and a flame ionization detector (Ni_{cat}-FID). Additionally, in the MPI-BGC, the $\delta^{13}C$–CO_2 of the air in the flasks was measured in the BGC IsoLab using a fully automated cryogenic extraction line (BGC-AirTrap) coupled to the dual-inlet system of a Finnigan MAT 252 stable isotope ratio mass spectrometer (IRMS, Thermo Fisher Scientific, Bremen, Germany) (Heimann et al., 2022). Calibration was performed against the international Jena Reference Air Set (JRAS-06) scale (Wendeberg et al., 2013). The $\delta^{13}C$ (of CO_2) corresponds to

$$\delta^{13}C = \left(\frac{\left(\frac{^{13}C}{^{12}C}\right)_{\text{sample}}}{\left(\frac{^{13}C}{^{12}C}\right)_{\text{standard}}} - 1 \right) \times 1000\ [‰]. \quad (1)$$

The $\Delta^{14}C$ notation is used to express the isotopic ratio $^{14}C/C$, with a correction for mass-dependent fractionation and radioactive decay. Specifically,

$$\Delta^{14}C = \left(F^{14}C\, e^{\lambda(1950 - y_{\text{meas}})} - 1 \right) \times 1000\ [‰], \quad (2)$$

where $F^{14}C$ ($= \frac{A_{SN}}{A_{ON}}$) is the fraction modern, with A_{SN} being the specific activity of the sample and A_{ON} being the specific activity of oxalic acid standard material (OxII), both normalized to $\delta^{13}C = -25‰$ with respect to the V-PDB standard; λ is the updated ^{14}C decay constant ($\frac{1}{8267}\ yr^{-1}$); and y_{meas} is the year of measurement. $\Delta^{14}C$ is corrected for mass-dependent fractionation through AMS online $\delta^{13}C$, assuming ^{14}C fractionates approximately twice as much as ^{13}C (Stuiver and Polach, 1977; Reimer et al., 2004).

$\Delta^{14}C$ from CO_2 in the air samples collected in flasks was determined after cryogenic extraction of CO_2 in a vacuum line and its conversion to graphite, which is the target of the Cs sputtering in the AMS at both CEZA and MPI-BGC. At the ICOS-CRL facility, CO_2 extraction is performed using a dedicated automated extraction and graphitization line (EGL) (Lux, 2018). At MPI-BGC, the extraction of CO_2 for radiocarbon analysis follows the same principles as EGL. ^{14}C-to-C ratios at both CEZA and MPI-BGC are corrected for mass-dependent fractionation by $\delta^{13}C$ measurements in the AMS and are calibrated against oxalic acid standard material (OxII).

The $\Delta^{14}C$ values of the reference background (321 m a.g.l.) are based on radiometric analysis of radiocarbon from samples of CO_2 absorbed in a NaOH solution (Levin et al., 1980). $\Delta^{14}C$ values from the integrated air in NaOH samples were determined through low-level gas proportional counting at the Institute of Environmental Physics in Heidelberg, Germany (Kromer and Münnich, 1992). For samples collected in 2019, the year of measurement (y_{meas}, Eq. 2) for radiocarbon analysis was 2020, and for samples collected in 2021, y_{meas} was 2023.

2.4 End-member mixing analysis

The Keeling plot and Miller–Tans plot methods are based on two conservation equations. First, it is assumed that the concentration of CO_2 below a forest canopy ($[CO_2]_{can}$) is the mix of CO_2 from a tropospheric background ($[CO_2]_{trop}$)

and the CO_2 released from ecosystem respiration ($[CO_2]_{ER}$) (Eq. 3) (Keeling, 1958, 1961; Miller and Tans, 2003). Second, isotopic mixing in CO_2 below the canopy is proportional to the concentration of CO_2 in the tropospheric background and ecosystem respiration (Eq. 4) (Tans, 1980). These assumptions lead to the following equations:

$$[CO_2]_{can} = [CO_2]_{trop} + [CO_2]_{ER}, \quad (3)$$

$$R_{can} \times [CO_2]_{can} = R_{trop} \times [CO_2]_{trop} + R_{ER} \times [CO_2]_{ER}, \quad (4)$$

where R is the isotopic ratio of C in CO_2, expressed as $\delta^{13}C$ for the stable C isotopes and as $\Delta^{14}C$ or $F^{14}C$ for the ^{14}C isotope over total C.

Using the mass conservation of Eq. (3), Eq. (4) can be reduced to

$$R_{can} = \frac{[CO_2]_{trop}}{[CO_2]_{can}} \times (R_{trop} - R_{ER}) + R_{ER}. \quad (5)$$

Equation (5) is, in essence, a linear equation of the form $y = ax + b$, where the independent variable x is $\frac{1}{[CO_2]_{can}}$; y is the isotopic signature observed in the canopy R_{can}; $a = (R_{trop} - R_{ER})[CO_2]_{trop}$; and b, or, hereafter, the y intercept, is R_{ER}, i.e., the isotopic signature of CO_2 respired by the whole ecosystem. Using linear regression, the values of a and b can be obtained if the values of x and y are known. This approach for obtaining the isotopic signature of a source in a two-end-member mixing model is commonly known as the Keeling plot method (Keeling, 1958). In this study, we are particularly interested in the radiocarbon signature of ecosystem respiration, which we express as $\Delta^{14}C_{ER}$ (and $F^{14}C_{ER}$ in the Appendix).

Notice that Eq. (4) leads to the requirement that the background signal does not change over time (Eq. 5) (Keeling, 1958, 1961). Miller and Tans (2003) rearranged Eq. (4), obtaining the following equation:

$$R_{can} \times [CO_2]_{can} - R_{trop} \times [CO_2]_{trop} = R_{ER}([CO_2]_{can} - [CO_2]_{trop}). \quad (6)$$

This can also be expressed as a linear function where the intercept b equals zero. Here, x is $([CO_2]_{can} - [CO_2]_{trop})$, i.e., the difference between CO_2 concentrations below and above canopy; y is $R_{can} \times [CO_2]_{can} - R_{trop} \times [CO_2]_{trop}$; and the slope a is R_{ER}, i.e., the isotopic signature of ecosystem respiration.

Such rearrangement removes the requirement of a constant background over time in the Keeling plot approach. However, it becomes necessary to explicitly account for the background concentration and C isotope ratio values in Eq. (6).

The isotopic carbon signatures of ecosystem respiration ($\delta^{13}C_{ER}$ and $\Delta^{14}C_{ER}$) were estimated with both the Keeling and Miller–Tans approaches. Both end-member mixing models considered all the heights below and above the canopy, i.e., 4, 24, 79, and 321 m, and were not separated according to the time of day. The results of the analyses were estimated by linear regression fits with ordinary least squares (model-I regression) (Zobitz et al., 2006). We report the mean values, with 1 standard error (σ), of the intercept obtained by the regressions in the Keeling approach and of the slope of the regression in the Miller–Tans approach. In both cases, we also report the 95 % confidence interval (CI, ranging between percentiles 2.5 and 97.5).

Because of the correction for mass-dependent fractionation, both $\Delta^{14}C$ and $F^{14}C$ do not reflect the effects of isotope fractionation. The variations in the radiocarbon signature will be related to the age of the carbon.

2.5 Conversion to mean transit time and reference atmospheric radiocarbon

To obtain a mean transit time from the estimated ^{14}C signature of ecosystem respiration, it is necessary to use atmospheric radiocarbon data as a reference. We used a compilation of recently reported data from the CORSO project as a reference for the atmospheric radiocarbon data in our study region, which include time series of atmospheric radiocarbon measured at research stations in the tropical region and surroundings. The data used for the conversion of $\Delta^{14}C_{ER}$ into mean transit time included the stations BHD (Baring Head, Aotearoa / New Zealand), CGO (Cape Grim, Australia), MER (Mérida Observatory, Venezuela) and SMO (Cape Matatula, Samoa) (Graven et al., 2012; Turnbull et al., 2017; Levin et al., 2010, 2022). The data were smoothed using curve fitting methods applied to time series in NOAA/ESRL/GMD (https://gml.noaa.gov/ccgg/mbl/crvfit/crvfit.html, last access: 15 December 2023) (Thoning et al., 1989), accounting for interannual variability, and this is reported in decimal years. The atmospheric $\Delta^{14}C$–CO_2 was averaged by year to have one value of $\Delta^{14}C$–CO_2 per year for the comparison with the year of collection of samples. The CORSO data are available in the Heidelberg University repository (https://heibox.uni-heidelberg.de/d/1f481155f63c46a8aaf0/, last access: 21 November 2023), and the CORSO report, with details of the collection and filtering of data, is available on the ICOS Carbon Portal (https://meta.icos-cp.eu/objects/HnpnYFcQljQ-SJer66F-hr-b, last access: 21 November 2023).

To estimate the time between C assimilation and release from the ecosystem (mean transit time), the $\Delta^{14}C_{ER}$ obtained from the intercept of the Keeling plot and the slope of the Miller–Tans plot was compared to the subset of the CORSO data described above. The difference between the year of collection of the samples and the equivalent calendar years where $\Delta^{14}C_{ER}$ = atmospheric $\Delta^{14}C$–CO_2 translates into an estimate of mean transit time in units of years (yr). When $\Delta^{14}C_{ER}$ is not equal to the atmospheric $\Delta^{14}C$–CO_2 of a given year, the calendar year with the closest atmospheric $\Delta^{14}C$–CO_2 to $\Delta^{14}C_{ER}$ is taken. Estimates of mean transit time are based on the variability of the mean $\Delta^{14}C_{ER} \pm \sigma$ (standard error of the linear regression), with

the 95 % confidence interval of the mean reported within parentheses.

2.6 Comparison with other approaches

The values of $\Delta^{14}C_{ER}$ obtained from end-member mixing analysis were converted to mean transit time and compared with predictions of two carbon balance models that can estimate the mean transit time of C in tropical ecosystems and with an estimate of the mean transit time produced from a synthesis of carbon and radiocarbon studies in the central Amazon region (Trumbore and De Camargo, 2009).

The first model is a simple one-pool model obtained as the total ecosystem C stock divided by the input GPP flux. This ratio provides an estimate of turnover time, as reported by Carvalhais et al. (2014) for tropical forests at the global scale. The assumption of a one-pool model with this turnover time results in a probability distribution of turnover times that follows an exponential distribution with a mean equal to the turnover time (Metzler and Sierra, 2018). Because, for a one-pool model, the age, turnover, and transit time of C are equal (Bolin and Rodhe, 1973; Sierra et al., 2017), we assume that this distribution of turnover times is equivalent to the distribution of transit times.

The second model is a multi-compartmental model developed for the Porce region of Colombia (Sierra et al., 2021b). This model tracks the movement of C across seven ecosystem compartments, namely foliage, fine litter, wood, coarse woody debris, fine roots, coarse roots, and soil carbon (0–30 cm). It produces estimates of the transit time distribution of carbon assuming a constant GPP input flux of $24 \pm 2\,\mathrm{Mg\,C\,ha^{-1}\,yr^{-1}}$.

A third estimate of a transit time distribution of C for tropical forests was obtained from the synthesis of the carbon and radiocarbon studies of Trumbore and De Camargo (2009). These authors reported a mean age of ecosystem respired CO_2 of 3–7 years. Their estimate was based on respiration fluxes and the mean ages of C in CO_2 derived from the decomposition of wood and roots in addition to radiocarbon-based turnover times of soil carbon (Chambers et al., 2004; Vieira et al., 2005; Telles et al., 2003; Trumbore et al., 2006).

All computations were performed in the R environment (R v.4.2.2) using RStudio (version 2023.03.0+386).

3 Results

3.1 Keeling plots

We produced Keeling plots for both isotopes, $\delta^{13}C$–CO_2 and $\Delta^{14}C$–CO_2, and for the two separate sampling campaigns in 2019 and 2021. For $\delta^{13}C$–CO_2, the intercept of the Keeling plot yielded a value of $-27.8\,‰ \pm 0.3\,‰$ for October 2019 and a value of $-29.0\,‰ \pm 0.5\,‰$ for December 2021 (Fig. 1). The statistical fit of the data to the linear model was remarkably good, with the values of the R^2 coefficient being equal to 1.0.

The $\delta^{13}C_{ER}$ (i.e., y intercept) values obtained from the Keeling plots for October 2019 and December 2021 were significantly different (year predictor p value < 0.001). The daytime CO_2 range (i.e., the difference between minimum and maximum concentrations over all heights) was approximately 111 ppm in October 2019, and in December 2021, it was slightly lower at 92 ppm. During the nighttime, the CO_2 range was about 50 ppm in 2019 and 66 ppm in 2021 (Fig. S1 in the Supplement). The $\delta^{13}C$–CO_2 mean value during the nighttime was $-10.5\,‰$, which agrees well with the mean observed in 2019. The daytime mean $\delta^{13}C$–CO_2 was more enriched in the heavier isotope ($-9.3\,‰$) based on 13 daytime samples in 2019 and 4 daytime samples in 2021. Minimum values of $\delta^{13}C$–CO_2 during the daytime and nighttime are, nevertheless, very similar ($-11.5\,‰$ and $-11.6\,‰$, respectively).

Variability during the daytime and nighttime and between sampling campaigns was much more pronounced for radiocarbon (Fig. 2) than for $\delta^{13}C$–CO_2. The statistical fit of the linear regression of the Keeling plot was relatively low for radiocarbon ($R^2 = 0.39$ in 2019 and 0.59 in 2021), although the obtained values of the intercepts were statistically significant (p values $= 0.005$ and 0.010 for 2019 and 2021, respectively).

$\Delta^{14}C$–CO_2 comprised a larger range of values in the second campaign, including more negative values at 24 m and a higher maximum ($18.4\,‰ \pm 2.3\,‰$) occurring during the daytime (Fig. 2). The minimum $\Delta^{14}C$–CO_2 during the daytime was $-2.5\,‰ \pm 2.2\,‰$, while, during the nighttime, it was $-4.8\,‰ \pm 2.2\,‰$, both measured at 24 m. However, the ΔCO_2 was smaller in the second campaign, which implied a larger error in the Keeling plot, as a consequence of the extended extrapolation to obtain the y intercept. The $\Delta^{14}C_{ER}$ mean values and standard error were $33\,‰ \pm 8\,‰$ and $74\,‰ \pm 21\,‰$ in October 2019 and December 2021, respectively (Fig. 3).

3.2 Miller–Tans model

The background CO_2 concentration for October 2019 was 408.2 ppm ($\sigma = 2.2$ ppm) based on two flasks collected at 79 m in the afternoon because flask sampling at 321 m started only in 2021. The background CO_2 concentration for December 2021 was 426.4 ppm ($\sigma = 0.002$ ppm) based on one flask collected at 321 m. Based on continuous measurements in 2022, a daily variation of CO_2 is estimated to be approximately 34 ppm at 81 m and approximately 14 ppm at 321 m (Fig. S2).

Alongside the small variation in the CO_2 concentrations at 79 m in 2019, $\delta^{13}C$–CO_2 varied from $-8.5\,‰$ to $-8.7\,‰$. Nevertheless, the estimates of $\delta^{13}C_{ER}$ are not significantly different between Keeling and Miller–Tans approaches despite the explicit incorporation of background variations in

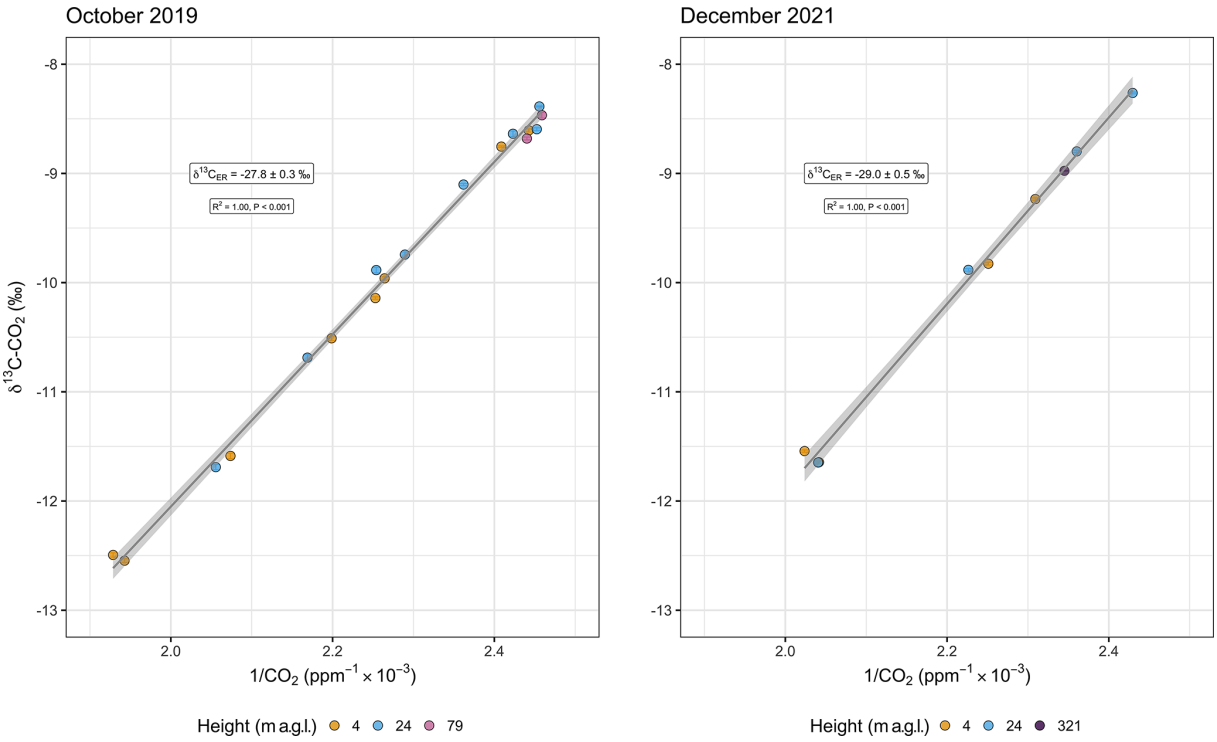

Figure 1. Keeling plot of δ^{13}C–CO_2 from below-canopy (4 and 24 m a.g.l.) and above-canopy (79 m a.g.l.) air for 5–6 October 2019 and 19–20 December 2021. The y intercept ($\delta^{13}C_{ER}$) changes from $-27.8\,‰ \pm 0.3\,‰$ to $-29.0\,‰ \pm 0.5\,‰$. Analytical errors of δ^{13}C–CO_2 ranged from 0.005 ‰ to 0.04 ‰. Similarly, analytical errors of CO_2 vary between 0.01 and 0.3 ppm. Therefore, error bars are not easily visible in this scale.

the latter method, remaining at around $-27.8\,‰ \pm 0.3\,‰$ for October 2019 and $-29.0\,‰ \pm 0.5\,‰$ for December 2021 (Miller–Tans plot not shown for δ^{13}C–CO_2).

Background Δ^{14}C–CO_2 is based on 1-month-integrated samples. For the campaign of October 2019, we used a sample collected between 9 September 2019 and 15 October 2019, with a Δ^{14}C–CO_2 of $8\,‰ \pm 2\,‰$. For the December 2021 campaign, two samples collected between 24 November 2021 and 26 January 2022, were averaged, providing a Δ^{14}C–CO_2 equal to $0\,‰ \pm 2\,‰$ (unpublished data). The Miller–Tans-based mean $\Delta^{14}C_{ER} \pm 1\sigma$ was $32\,‰ \pm 8\,‰$ (15 ‰–48 ‰, 95 % CI) in October 2019 and $78\,‰ \pm 24\,‰$ (21 ‰–135 ‰, 95 % CI) in December 2021 (Fig. 4). Estimates in F^{14}C are given in the Appendix (Fig. A1).

3.3 Estimates of mean transit time and comparison to other values from the literature

Our values of $\Delta^{14}C_{ER}$ obtained through end-member mixing analysis were compared with radiocarbon atmospheric records to estimate the mean age of the respired CO_2 – in other words, the mean transit time of carbon.

The Keeling plot for the campaign in October 2019 results in a mean $\Delta^{14}C_{ER}$ of 33 ‰, with a standard error of 8 ‰ (17 ‰–50 ‰, 95 % CI), which corresponds to the atmospheric Δ^{14}C–CO_2 of the years 2015 to 2011 CE (common era) (2017 to 2008 CE, 95 % CI) based on the CORSO data. Thus, the corresponding mean age of respired CO_2 for the samples collected in October 2019, i.e., 2019 minus 2015 and 2019 minus 2011, is 4–8 years (2–11 years, 95 % CI). The $\Delta^{14}C_{ER}$ based on the samples collected in December 2021 corresponds to the atmospheric Δ^{14}C–CO_2 of the years 2007 to 1999 CE (2015 to 1994 CE, 95 % CI), which corresponds to a mean age of ecosystem respiration of 14–22 years (6–27 years, 95 % CI).

The Miller–Tans approach for the campaign in October 2019 results in a $\Delta^{14}C_{ER}$ range that corresponds to the atmospheric Δ^{14}C–CO_2 of the years 2015 to 2011 CE (2017 to 2009 CE, 95 % CI) based on the CORSO data, i.e., a similar range as the Keeling plots. Thus, the corresponding mean age of respired CO_2 for the samples collected in October 2019 by the Miller–Tans approach is 4–8 years (2–10 years, 95 % CI). The $\Delta^{14}C_{ER}$ based on the samples collected in December 2021 corresponds to the atmospheric Δ^{14}C–CO_2 of the years 2007 to 1998 CE (2016 to 1993 CE, 95 % CI), which corresponds to a mean age of ecosystem respiration of 14–23 years (5–28 years, 95 % CI).

Estimates of the mean transit time of tropical ecosystems are available from three other approaches (Table 1). In the first approach (where turnover time equates to stock over flux), Carvalhais et al. (2014) reported a mean turnover time

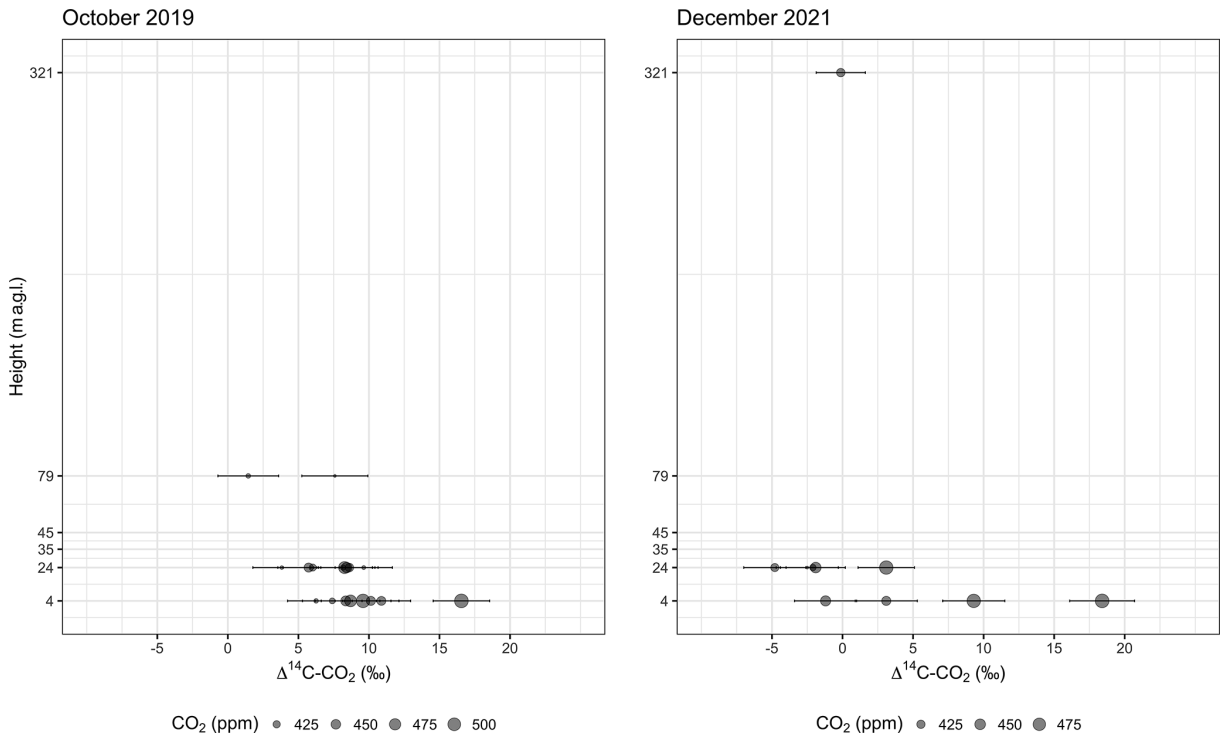

Figure 2. Distribution of values of $\Delta^{14}C$–CO_2 and CO_2 concentrations according to the sampling heights below (4 and 24 m a.g.l.) and above (79 and 321 m a.g.l.) the canopy. The canopy level in the study plot is around 35 m, and some emergent trees occur at 45 m height. The CO_2 concentration at 321 m is based on measurements from a flask, and the $\Delta^{14}C$ value is the average between two integrated samples (see main text). Analytical errors of $\Delta^{14}C$–CO_2 measurements vary between 1.7 ‰ and 2.3 ‰.

of 14 years (12–18 years, 95 % CI), obtained as the ratio of the total C stock to GPP for tropical forests. It represents the mean of an exponentially distributed transit time distribution (Metzler and Sierra, 2018).

In a multi-compartmental approach, the transit time distribution reported from a seven-pool model for the Porce region of Colombia has a mean value of 11 ± 1 years (Sierra et al., 2021b).

Based on a synthesis of carbon and radiocarbon data, Trumbore and De Camargo (2009) reported an average age of respired CO_2 weighted by the fluxes of different compartments (e.g., litter, wood) that ranged from 3 to 7 years for central Amazon forests near Manaus.

4 Discussion

4.1 What is the mean transit time of C for an Amazon terra firme forest estimated with Keeling and Miller–Tans plots of $^{14}CO_2$?

We estimated the mean transit time of C for a tropical forest ecosystem using Keeling and Miller–Tans plots from field measurements of ^{14}C–CO_2. Although Keeling plots have been successfully used over decades to characterize the $\delta^{13}C$ signature of ecosystem respiration (e.g., Ehleringer and Cook, 1998; Knohl et al., 2005; de Araújo et al., 2008; Mauritz et al., 2019), the method has rarely been used with $^{14}CO_2$. The Miller–Tans approach with radiocarbon was used previously to understand biogenic and fossil sources contributing to the atmospheric air in urban environments (Miller et al., 2020). To our knowledge, the study of Phillips et al. (2015) was the first that combined isotope mixing analysis with $^{14}CO_2$ measurements to estimate the age of respired carbon in a temperate forest ecosystem.

Our approach provided estimates of mean transit time in a range from 2 to 28 years (95 % CI), differing depending on the sampling campaign. These estimates of mean transit time suggest that the carbon fixed during photosynthesis in these tropical forests is respired, on average, within 1 to 3 decades. The $\delta^{13}C_{ER}$ estimated through the Keeling plot is equal to the estimate obtained through the Miller–Tans plot (where the background is explicitly incorporated). The similarity of $\delta^{13}C_{ER}$ estimates in both methods suggests that the small variations in CO_2 concentrations and $\delta^{13}C$–CO_2 at 79 m were small enough not to violate the implicit assumption of a stable background in the Keeling plot method. The results of $\delta^{13}C_{ER}$ suggest that the source of ecosystem respiration has shifted between the two sampling campaigns from a value of $-27.8 ‰ \pm 0.3 ‰$ in 2019 to a more depleted value of $-29.0 ‰ \pm 0.5 ‰$ in 2021 ($p < 0.001$ with the year

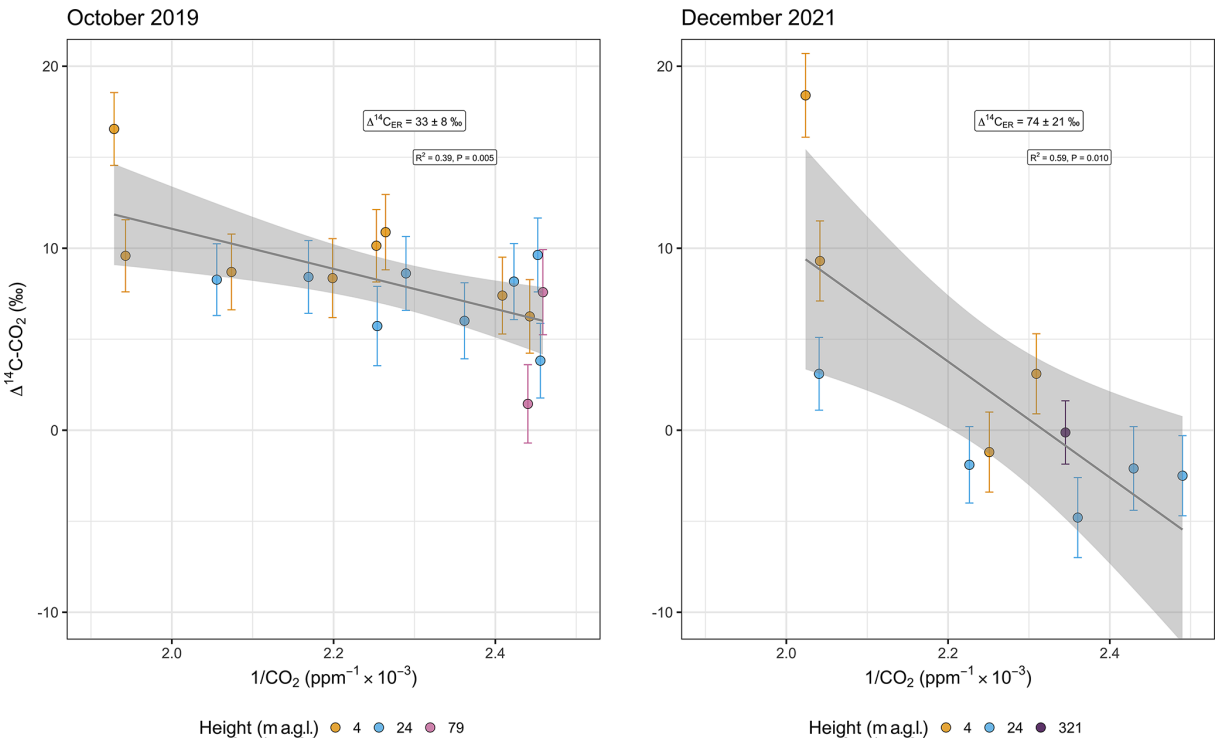

Figure 3. Keeling plot of $\Delta^{14}C$–CO_2 for sampling campaigns in October 2019 and December 2021. $\Delta^{14}C_{ER}$ values change from 33 ‰ ± 8 ‰ to 74 ‰ ± 21 ‰. The light-gray ribbon represents the 95 % confidence interval of the predictions.

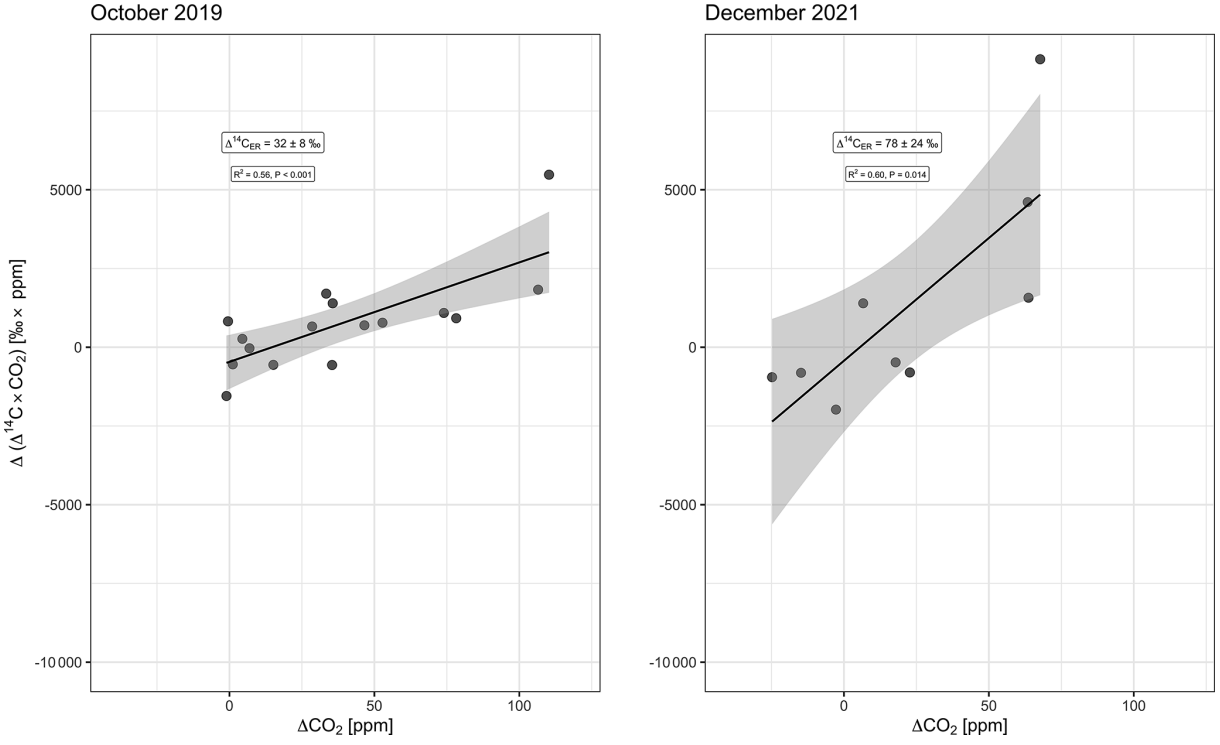

Figure 4. Miller–Tans model (with ordinary least squares regression) for October 2019 and December 2021. The light-gray ribbon represents the 95 % confidence interval.

Table 1. Estimates of mean transit time of C for ATTO for the years 2019 and 2021 based on the conversion of $\Delta^{14}C_{ER}$ (mean values $\pm\sigma$) into mean transit time of carbon. The mean transit time based on the 95 % CI range is presented within parentheses. Comparison between different approaches, namely the end-member mixing analyses of this study at the ATTO site (Keeling plot and Miller–Tans plot), and estimates for other sites and tropical regions. For steady-state systems, the estimate of the mean transit time of C does not change with the year. The turnover time is as estimated by Carvalhais et al. (2014). The seven-pool model was computed by Sierra et al. (2021b). The data synthesis was done by Trumbore and De Camargo (2009).

		Mean transit time (95 % CI) [years]	
Method	Study site	October 2019	December 2021
Keeling plot	ATTO site, Brazil	4–8 (2–11)	14–22 (6–27)
Miller–Tans plot	ATTO site, Brazil	4–8 (2–10)	14–23 (5–28)
Turnover time	Tropical forests, worldwide	14 (12–18)	
Seven-pool model	Porce region, Colombia	10–12	
Data synthesis	Central Amazon, Brazil	3–7	

as a predictor). These changes in $\delta^{13}C$–CO_2 are known to occur in the Amazon region due to changes in precipitation (Ometto et al., 2002; Pataki et al., 2003). Assuming that the environmental factors altering $\delta^{13}C$–CO_2 are also responsible for the changes in the $\Delta^{14}C$–CO_2, the observed difference in $\delta^{13}C_{ER}$ may help to explain the differences in mean transit time that we observed among the two field campaigns. Changes in other environmental factors such as soil moisture may have also contributed to this difference in mean transit times. Chambers et al. (2004) have demonstrated that, for example, high soil respiration fluxes correlate with low soil moisture levels in the central Amazon. Furthermore, changes in the composition of pools contributing to respired C can alter its C transit time (Lu et al., 2018). Meteorological data from the 80 m walk-up tower show that precipitation and soil water content were higher during the campaign of December 2021 than in the campaign of October 2019 (Figs. S4 and S6).

Allowing the background to vary (Miller–Tans approach) requires knowing the values of the $\Delta^{14}C$–CO_2 and CO_2 concentrations during the sampling period. In this study, we used a few afternoon samples from the height of 79 m a.g.l., which, despite being reasonable, may still not be the best option for our fits, especially because it does not cover the whole sampling period. The measurements from 321 m a.g.l. are closer to an actual background; however, the resolution of 1 month in those samples could impair our ability to distinguish small variations that we may have captured in our 2 d campaigns.

Moreover, the estimate of mean transit time is done by comparison with long-term records of $\Delta^{14}C$–CO_2 in the background atmosphere. This implies the need for a time series of $\Delta^{14}C$–CO_2 that is representative of the study region. Even though the division of regions in the bomb curve (Hua et al., 2022) is a useful guide, direct measurements of $\Delta^{14}C$–CO_2 are still largely lacking in the Amazon region. Moreover, the atmospheric dynamics over the Amazon Basin are not trivial (Ancapichún et al., 2021), and the location of ATTO is influenced by mixed sources throughout the year (Botía et al., 2022).

Based on back-trajectory footprint analysis, the air circulation over ATTO between 80 and 1000 m a.s.l. is highly influenced by the oscillation of the Intertropical Convergence Zone (ITCZ). During the wet season (February–May), the air masses predominantly follow a northeastern path, while, during the dry season (August–November), the dominant wind directions come from the southeast, where the arc of deforestation is located in Brazil (Pöhlker et al., 2019; Saturno et al., 2018). The ITCZ also influences the air movement over ATTO during the dry-to-wet (December–January) and wet-to-dry (June–July) seasons, making the ATTO site meteorologically located in the Northern Hemisphere (NH) during the former and meteorologically located in the Southern Hemisphere (SH) during the latter (Andreae et al., 2015). According to the division of zones proposed by Hua et al. (2022), which also takes into account the ITCZ patterns, the ATTO site would be located in SH Zone 3. However, the patterns of air movement above the central Amazon suggest that a mixed curve (Marsh et al., 2018) must be more appropriate when estimating mean transit times based on $\Delta^{14}C$–CO_2 in the central Amazon.

Keeling plots of $\Delta^{14}C$–CO_2 (where no background subtraction is applied) differ from the Miller–Tans approach by a few per mille, which corresponds to 1 to 2 years in mean transit time considering a steady annual decline of 3 ‰ to 5 ‰ in atmospheric $\Delta^{14}C$–CO_2. This indicates that choosing between Keeling and Miller–Tans approaches for estimating the $\Delta^{14}C_{ER}$ is not the main factor impacting the precision and accuracy of the mean transit time estimate based on observations of ^{14}C–CO_2 in a vertical subcanopy profile. The sample size and uncertainty of C isotopic ratio measurements may have a larger influence on the standard errors of the y intercept and slope of the regression lines in the Keeling plot and Miller–Tans plot, respectively. The method of employing end-member mixing analysis to $^{14}CO_2$ measurements thus also seems promising for the tropical regions alongside

the temperate regions, as demonstrated before by Phillips et al. (2015). Nevertheless, more work is needed to repeat the measurements with seasonal frequency in the Amazonian region and to obtain similar estimates in other tropical regions worldwide. Additional estimates of empirical mean transit time would better quantify spatial and temporal variations in the C mean transit time. Furthermore, they would help to understand whether variations in the mean transit time are due to interannual variability or a trend in shifting mean transit times in tropical terrestrial ecosystems (Sierra et al., 2023).

4.2 How does this empirical mean transit time compare to model estimates of transit time in the Amazon region?

We compared our observation-based results with three previous estimates of mean transit time for tropical forests: the apparent turnover time estimated by Carvalhais et al. (2014) from GPP and total carbon stocks, the estimate of the age of respired carbon from a synthesis of observations reported by Trumbore and De Camargo (2009) for the central Amazon region, and the mean value of a transit time distribution computed with a seven-pool model for the Porce region of Colombia (Sierra et al., 2021b; Chanca et al., 2022).

In two short campaigns such as ours, the observed increase in the radiocarbon signature may be related to a short-term increase in the flux of one of the older respiration sources. Potential sources of radiocarbon that could be relevant due to being large enough and having high enough radiocarbon contents are dead wood (either as standing dead trees or as coarse woody debris) or old soil organic matter that gets destabilized with high water contents during the rainy season. For the ATTO site, there is good evidence that shows strong differences in temperature, precipitation, solar radiation, and soil water content between the two sampling campaigns (Figs. S3–S6), which may help to explain differences in transit times.

To evaluate changes in the isotopic signature of the main ER sources, the $\delta^{13}C_{ER}$ was estimated through Keeling plots using the same samples. The $\delta^{13}C_{ER}$ showed a smaller variation than $\Delta^{14}C_{ER}$, being $-27.8‰ \pm 0.3‰$ in October 2019 and $-29.0‰ \pm 0.5‰$ in December 2021. A similar variability in $\delta^{13}C_{ER}$ has been observed in a topographical gradient at the Reserva Cueiras, a site in the central Amazon approximately 80 km away from ATTO (de Araújo et al., 2008). In that case, the valleys presented more negative $\delta^{13}C_{ER}$ values than the plateau areas during the dry season. The variability observed by de Araújo et al. (2008) indicated a correlation between $\delta^{13}C_{ER}$ and the water vapor saturation deficit in the air (D), which was more evident on the plateaus than on the valleys. In their study, a $\delta^{13}C_{ER}$ about 1 ‰–1.5 ‰ lighter was linked to a high D with low soil water contents, which resembles our campaign of October 2019 in comparison to December 2021.

Our data are spatially and temporally limited. Although the observed difference in $\delta^{13}C_{ER}$ is statistically significant, it is not possible to set apart the effects of seasonal variability or changes on the fluxes of the respiration sources on the C isotopic signatures. Hence, the observed differences in $\Delta^{14}C_{ER}$ and, thus, mean transit time might be related to seasonal variabilities that cannot be fully assessed with sporadic campaigns. To effectively elucidate the underlying drivers of the variability in the mean transit time, more ecosystem respiration sampling for radiocarbon measurements (and $\delta^{13}C$ as the ancillary) is needed.

The mean transit time for the campaign in 2021 agrees with the turnover time estimated by Carvalhais et al. (2014); however, the same does not hold for the campaign in 2019, when the mean transit time based on end-member mixing analysis is shorter. The approach of Carvalhais et al. (2014) to obtain a turnover time integrates over large temporal and spatial scales by incorporating gross primary production values and C stocks over several years and with a resolution of 0.5°. However, it does not discern between pools of different ages that contribute in varied proportions to the total respiration flux. Therefore, it cannot account for pools with different $\Delta^{14}C$ but can only approximate the radiocarbon signature within a well-mixed total ecosystem respiration. Moreover, some of the potential reasons for the mismatch in 2019 include a seasonal variability of $\Delta^{14}C$–CO_2 in the central Amazon, different contributions of respiration sources from year to year due to climate variations, or even a poor representation of local measurements in a short-term campaign in comparison to the dynamics of the whole Amazon rainforest. More studies conducted in different seasons, targeting individual respiration sources, and covering larger temporal and spatial scales are needed to overcome these different possibilities. The comparison with other estimates of mean transit time, however, suggests that this metric might not be constant over time, even for old-growth forests in the central Amazon.

In contrast, in sites close to Manaus, Trumbore and De Camargo (2009) estimated a mean transit time of 3 to 7 years, which is similar to the value obtained in this study if we consider only the campaign of October 2019. The $\Delta^{14}C_{ER}$ of the second campaign (December 2021) generates a mean transit time of about 14 to 23 years, which is about 3 times higher than the estimate by Trumbore and De Camargo (2009) for the central Amazon; however, this is similar to the age estimate of 24 years by Fung et al. (1997) for heterotrophically respired C in broad-leaved evergreen tropical forests, also cited by Trumbore and De Camargo (2009). However, the model used by Fung et al. (1997) assumed that 50 % of C was respired autotrophically, with one-third of the remaining 50 % being allocated to leaves, one-third being allocated to stems, and one-third being allocated to roots. In contrast, the study of respiration fluxes (Chambers et al., 2004) demonstrated that autotrophic respiration returned 70 % of the C assimilated by a central Amazon rainforest to the atmosphere; thus, we expect the transit time estimate of Fung

et al. (1997) to be systematically too long. The estimates of Trumbore and De Camargo (2009) were based on respiration fluxes, mean ages of C in decomposing wood and roots, and turnover times of soils based on radiocarbon data (Chambers et al., 2004; Vieira et al., 2005; Telles et al., 2003; Trumbore et al., 2006). Such information was summarized into an estimate of the mean time lag between photosynthetic assimilation and ecosystem C release through respiration. This time lag can be compared to our estimate of mean transit time based on $\Delta^{14}C_{ER}$ as both are defined similarly and either intrinsically or explicitly incorporate the path of C through multiple interconnected pools with different turnover times.

A seven-pool model developed for a tropical forest in Colombia (Porce model) has a mean transit time of 10 to 12 years (Sierra et al., 2021b), which falls in between the mean transit time we estimated for October 2019 and December 2021. Therefore, it suggests that a multi-compartmental model estimates an average of the differences or trends of the ecosystem's mean transit time. The Porce model accounts for the C composition and C age structure of different compartments. A similar model for the central Amazon could be parameterized to account for the potential respiration sources that could drive the radiocarbon isotopic signature of ecosystem respiration by being large enough and by having high radiocarbon contents, such as dead wood (Chambers et al., 2004). This way, the empirical estimate of mean transit time can help to constrain a multi-compartmental model that is more representative of the central Amazon forest.

Our analysis shows that an empirical mean transit time based on forest air $\Delta^{14}C$–CO_2 coupled to isotope mixing analysis compares well with model estimates and other experimental approaches, at least for tropical forests. The differences from one year to the other or even between seasons imply a potential natural variability in the weights of fluxes from different C pools, with large differences in their turnover times. This variability could influence the C balance calculation in Amazon forests more than previously thought. In this sense, a practical method to calculate an ecosystem time metric such as transit time might improve our understanding of the C balance in Amazon forests and their role as C sources and sinks of atmospheric CO_2. This method also has the resolution to tackle temporal and spatial variabilities of the mean transit time of ecosystem respiration.

5 Conclusions

We obtained, for the first time in a tropical forest, an empirical estimate of a mean transit time of the carbon of ecosystem respiration based on end-member mixing analysis of radiocarbon measurements of ambient and atmospheric CO_2. We estimate the mean transit time of carbon for a plateau area of a near-pristine central Amazon forest, ranging from 1 to almost 3 decades. Our results suggest that a potentially large proportion of carbon assimilated through photosynthesis is released back to the atmosphere relatively quickly. This could affect interpretations of the role of Amazon forests as a C sink or source.

Our results also showed that the age of respired carbon may be highly dynamic, with important changes among seasons or years. This is in contrast to model-based estimates of transit time that often make the assumption of equilibrium and therefore cannot predict a time-dependent mean transit time. Potential reasons for the variability of transit times include (i) natural variation of ecosystem processes due to the seasonality and inter-annual variability of environmental factors (e.g., changes in precipitation), (ii) human activities such as fire that release old carbon and affect atmospheric $\Delta^{14}C$–CO_2, and (iii) high spatial and temporal heterogeneity in the sources of respired C at the ecosystem level. Hence, it is essential to monitor the mean transit time of tropical ecosystems because it can change over time. Additionally, studies exploring the $^{14}CO_2$ respired by different components can help to define the underlying distribution of the transit time of C that can have its mean value compared to the empirical estimate obtained through end-member mixing analysis.

The method presented here was scarcely employed in the past and was non-existent as applied to an Amazon forest. However, this method has large potential for understanding not only the source of respired carbon but also its age and the speed at which carbon is assimilated and respired by forest organisms. The method is particularly useful in tropical forests because of the large gradients and diurnal variations in the CO_2 concentration and its $\Delta^{14}C$ in the dense forest canopy. We showed that our sampling design was effective in obtaining a meaningful mean transit time of C with observations and isotope mixing analysis. Our mean transit time also compares well to other previous estimates based on model or data syntheses.

Appendix A: End-member mixing models with $F^{14}C$ notation

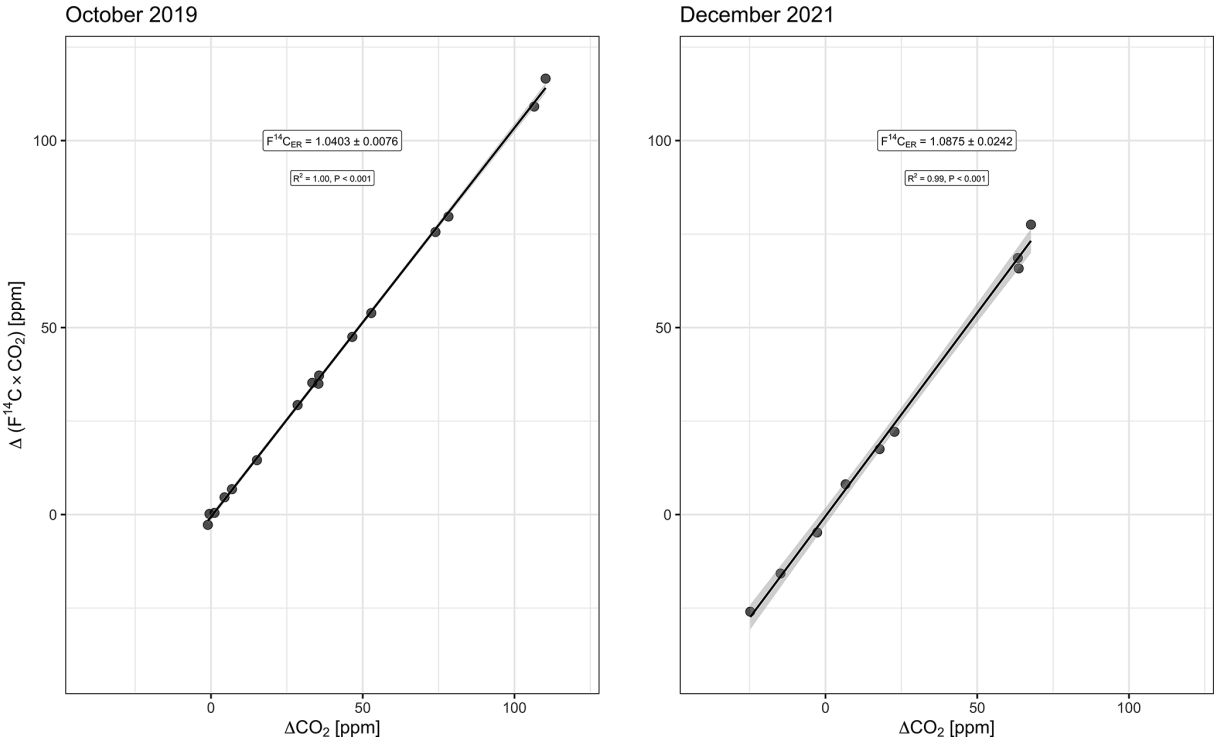

Figure A1. Miller–Tans model (with ordinary least squares regression) for October 2019 and December 2021. Slope of the regression line is the radiocarbon isotopic signature of the ecosystem respiration in $F^{14}C$ notation, i.e., $F^{14}C_{ER}$. $F^{14}C_{ER} = 1.0403 \pm 0.0076$ in October 2019 and $F^{14}C_{ER} = 1.0875 \pm 0.0242$ in December 2021. The light-gray ribbon represents the 95 % confidence interval.

In other studies using Miller–Tans plots of $\Delta^{14}C$–CO_2, the context of interest has been to determine the fossil fraction in CO_2 emissions in urban areas (e.g., Miller et al., 2020). In such contexts, $\Delta^{14}C$–CO_2 has values that are always below zero (down to -1000 ‰ if 100 % fossil). On the other hand, ecosystem respiration can have a variety of $\Delta^{14}C$–CO_2 values, linked to the varied radiocarbon signatures of its sources. Therefore, in the context of this study, $\Delta^{14}C$–CO_2 can be positive (e.g., decomposition of old carbon with bomb signature), negative (pre-bomb or contemporaneous atmosphere), and zero (when the atmospheric value crosses from the bomb ^{14}C signature to natural levels). In the Miller–Tans plots, the y axis is the product of the C isotopic ratio by the CO_2 concentration (of the subcanopy values minus the background value) (Eq. 6). Thus, in $\Delta^{14}C$ notation, a data point with a y value equal to zero can be a consequence of (i) a subcanopy combination ($\Delta^{14}C \times CO_2$) equal to the current atmosphere or (ii) simply a $\Delta^{14}C$ equal to zero. Such ambiguity does not occur when $F^{14}C$ is used instead because $F^{14}C$ can only assume positive values. Calculating the Miller–Tans plot with $F^{14}C$ or $\Delta^{14}C$ does not change the value of the slope of the regression line; therefore, it does not change the estimate of the mean transit time.

Data availability. The CORSO data are available in the Heidelberg University repository (https://heibox.uni-heidelberg.de/d/1f481155f63c46a8aaf0/, Hammer and Levin, 2023a), and the CORSO report with details of the collection and filtering of data is available on the ICOS Carbon Portal (https://meta.icos-cp.eu/objects/HnpnYFcQljQ-SJer66F-hr-b, Hammer and Levin, 2023b). The analytical results of the flasks collected for this work are available on the ATTO data portal (https://www.attodata.org/, last access: 15 November 2024) under the ID no. 437 (https://doi.org/10.17871/atto.437.4.1683, Chanca et al., 2024a) for the flasks collected in October 2019 and under the ID no. 438 (https://doi.org/10.17871/atto.438.4.1684, Chanca et al., 2024b) for the flasks collected in December 2021.

Supplement. The supplement related to this article is available online at: https://doi.org/10.5194/bg-22-455-2025-supplement.

Author contributions. IC: conceptualization, data curation, formal analysis, investigation, methodology, project administration, validation, visualization, writing (original draft preparation, review and editing). IL: conceptualization, data curation, formal analysis, funding acquisition, methodology, resources, supervision, validation,

writing (review and editing). ST: funding acquisition, project administration, resources, supervision, writing (review and editing). KM: resources, supervision, writing (review and editing). JL: data curation, funding acquisition, methodology, resources, validation, writing (review and editing). CAQ: funding acquisition, project administration, resources, writing (review and editing). ACdA: data curation, formal analysis, resources, validation, visualization, writing (review and editing). CQDJ: data curation, formal analysis, resources, validation, visualization, writing (review and editing). HvA: data curation, formal analysis, resources, validation, visualization, writing (review and editing). SH: data curation, resources, validation, writing (review and editing). CAS: conceptualization, formal analysis, funding acquisition, methodology, project administration, resources, supervision, writing (review and editing).

Competing interests. The contact author has declared that none of the authors has any competing interests.

Disclaimer. Publisher's note: Copernicus Publications remains neutral with regard to jurisdictional claims made in the text, published maps, institutional affiliations, or any other geographical representation in this paper. While Copernicus Publications makes every effort to include appropriate place names, the final responsibility lies with the authors.

Acknowledgements. This work would not have been possible without the contribution and support of Ingeborg Levin (R.I.P.), who was working with us on finalizing the paper at the time of her death. All meetings and communications with her contributed to the definition of the experimental design, understanding of radiocarbon background data, interpretation of the results, and several other aspects of this work. She is immortalized in the radiocarbon community for her wisdom, contributions, and endless support to the ones who had the honor of meeting her. Her support to the first author goes beyond the scientific realm and this Acknowledgements section. The authors would also like to give thanks for all the support provided by the ATTO team at the research site regarding the logistics of the transportation of material. Special thanks are given to Roberta Pereira de Souza, Yago Rodrigues Santos, Antônio Huxley Melo Nascimento, Amaury Rodrigues Pereira, and Nagib Alberto de Castro Souza. We would also like to thank the personnel from ICOS-CRL and the central laboratories of the MPI-BGC, particularly Axel Steinhof, Heike Machts, Heiko Moossen, Michael Rothe, Armin Jordan, and Steffen Knabe. The authors would like to thank the Brazilian funding agencies of the Brazilian National Council for Science and Technology and FAPERJ – Fundação Carlos Chagas Filho de Amparo à Pesquisa do Estado do Rio de Janeiro for the grants awarded to Kita Damasio Macario (grant nos. CNPq 317397/2021-4 and FAPERJ E-26/200.540/2023). We are also grateful for the INCT-FNA support (grant no. 464898/2014-5). This work and the Amazon Tall Tower Observatory (ATTO) project were funded by the German Federal Ministry of Education and Research (grant no. 01 LK 1602 C and 01 LK 2101 A) and the Max Planck Society.

Financial support. This research has been supported by the Bundesministerium für Bildung und Forschung (BMBF, grant nos. 01 LK 1602 C and 01 LK 2101 A); the Brazilian National Council for Science and Technology (CNPq, grant no. 317397/2021-4); the Brazilian Fundação Carlos Chagas Filho de Amparo à Pesquisa do Estado do Rio de Janeiro (FAPERJ, grant no. E-26/200.540/2023); the Brazilian Instituto Nacional de Ciência e Tecnologia: Física Nuclear e Aplicações (INCT-FNA, grant no. 464898/2014-5); and the Max Planck Society.

The article processing charges for this open-access publication were covered by the Max Planck Society.

Review statement. This paper was edited by Anja Rammig and reviewed by Karis McFarlane and one anonymous referee.

References

Ancapichún, S., De Pol-Holz, R., Christie, D. A., Santos, G. M., Collado-Fabbri, S., Garreaud, R., Lambert, F., Orfanoz-Cheuquelaf, A., Rojas, M., Southon, J., Turnbull, J. C., and Creasman, P. P.: Radiocarbon bomb-peak signal in tree-rings from the tropical Andes register low latitude atmospheric dynamics in the Southern Hemisphere, Sci. Total Environ., 774, 145126, https://doi.org/10.1016/j.scitotenv.2021.145126, 2021.

Andreae, M. O., Acevedo, O. C., Araùjo, A., Artaxo, P., Barbosa, C. G. G., Barbosa, H. M. J., Brito, J., Carbone, S., Chi, X., Cintra, B. B. L., da Silva, N. F., Dias, N. L., Dias-Júnior, C. Q., Ditas, F., Ditz, R., Godoi, A. F. L., Godoi, R. H. M., Heimann, M., Hoffmann, T., Kesselmeier, J., Könemann, T., Krüger, M. L., Lavric, J. V., Manzi, A. O., Lopes, A. P., Martins, D. L., Mikhailov, E. F., Moran-Zuloaga, D., Nelson, B. W., Nölscher, A. C., Santos Nogueira, D., Piedade, M. T. F., Pöhlker, C., Pöschl, U., Quesada, C. A., Rizzo, L. V., Ro, C.-U., Ruckteschler, N., Sá, L. D. A., de Oliveira Sá, M., Sales, C. B., dos Santos, R. M. N., Saturno, J., Schöngart, J., Sörgel, M., de Souza, C. M., de Souza, R. A. F., Su, H., Targhetta, N., Tóta, J., Trebs, I., Trumbore, S., van Eijck, A., Walter, D., Wang, Z., Weber, B., Williams, J., Winderlich, J., Wittmann, F., Wolff, S., and Yáñez-Serrano, A. M.: The Amazon Tall Tower Observatory (ATTO): overview of pilot measurements on ecosystem ecology, meteorology, trace gases, and aerosols, Atmos. Chem. Phys., 15, 10723–10776, https://doi.org/10.5194/acp-15-10723-2015, 2015.

Baker, J. C. and Spracklen, D. V.: Climate benefits of intact Amazon forests and the biophysical consequences of disturbance, Frontiers in Forests and Global Change, 2, 47, https://doi.org/10.3389/ffgc.2019.00047, 2019.

Beer, C., Reichstein, M., Tomelleri, E., Ciais, P., Jung, M., Carvalhais, N., Rödenbeck, C., Arain, M. A., Baldocchi, D., Bonan, G. B., Bondeau, A., Cescatti, A., Lasslop, G., Lindroth, A., Lomas, M., Luyssaert, S., Margolis, H., Oleson, K. W., Roupsard, O., Veenendaal, E., Viovy, N., Williams, C., Woodward, F. I., and Papale, D.: Terrestrial Gross Carbon Dioxide Uptake: Global Distribution and Covariation with Climate, Science, 329, 834–838, https://doi.org/10.1126/science.1184984, 2010.

Bolin, B. and Rodhe, H.: A note on the concepts of age distribution and transit time in natural reservoirs, Tellus, 25, 58–62, 1973.

Botía, S., Komiya, S., Marshall, J., Koch, T., Gałkowski, M., Lavric, J., Gomes-Alves, E., Walter, D., Fisch, G., Pinho, D. M., Nelson, B. W., Martins, G., Luijkx, I. T., Koren, G., Florentie, L., Carioca de Araújo, A., Sá, M., Andreae, M. O., Heimann, M., Peters, W., and Gerbig, C.: The CO_2 record at the Amazon Tall Tower Observatory: A new opportunity to study processes on seasonal and inter-annual scales, Global Change Biol., 28, 588–611, https://doi.org/10.1111/gcb.15905, 2022.

Brienen, R. J. W., Phillips, O. L., Feldpausch, T. R., Gloor, E., Baker, T. R., Lloyd, J., Lopez-Gonzalez, G., Monteagudo-Mendoza, A., Malhi, Y., Lewis, S. L., Vásquez Martinez, R., Alexiades, M., Álvarez Dávila, E., Alvarez-Loayza, P., Andrade, A., Aragão, L. E. O. C., Araujo-Murakami, A., Arets, E. J. M. M., Arroyo, L., Aymard C., G. A., Bánki, O. S., Baraloto, C., Barroso, J., Bonal, D., Boot, R. G. A., Camargo, J. L. C., Castilho, C. V., Chama, V., Chao, K. J., Chave, J., Comiskey, J. A., Cornejo Valverde, F., da Costa, L., de Oliveira, E. A., Di Fiore, A., Erwin, T. L., Fauset, S., Forsthofer, M., Galbraith, D. R., Grahame, E. S., Groot, N., Hérault, B., Higuchi, N., Honorio Coronado, E. N., Keeling, H., Killeen, T. J., Laurance, W. F., Laurance, S., Licona, J., Magnussen, W. E., Marimon, B. S., Marimon-Junior, B. H., Mendoza, C., Neill, D. A., Nogueira, E. M., Núñez, P., Pallqui Camacho, N. C., Parada, A., Pardo-Molina, G., Peacock, J., Peña-Claros, M., Pickavance, G. C., Pitman, N. C. A., Poorter, L., Prieto, A., Quesada, C. A., Ramírez, F., Ramírez-Angulo, H., Restrepo, Z., Roopsind, A., Rudas, A., Salomão, R. P., Schwarz, M., Silva, N., Silva-Espejo, J. E., Silveira, M., Stropp, J., Talbot, J., ter Steege, H., Teran-Aguilar, J., Terborgh, J., Thomas-Caesar, R., Toledo, M., Torello-Raventos, M., Umetsu, R. K., van der Heijden, G. M. F., van der Hout, P., Guimarães Vieira, I. C., Vieira, S. A., Vilanova, E., Vos, V. A., and Zagt, R. J.: Long-term decline of the Amazon carbon sink, Nature, 519, 344–348, https://doi.org/10.1038/nature14283, 2015.

Carvalhais, N., Forkel, M., Khomik, M., Bellarby, J., Jung, M., Migliavacca, M., Mu, M., Saatchi, S., Santoro, M., Thurner, M., Weber, U., Ahrens, B., Beer, C., Cescatti, A., Randerson, J. T., and Reichstein, M.: Global covariation of carbon turnover times with climate in terrestrial ecosystems, Nature, 514, 213–217, https://doi.org/10.1038/nature13731, 2014.

Chambers, J. Q., Tribuzy, E. S., Toledo, L. C., Crispim, B. F., Higuchi, N., dos Santos, J., Araújo, A. C., Kruijt, B., Nobre, A. D., and Trumbore, S. E.: Respiration from a tropical forest ecosystem: partitioning of sources and low carbon use efficiency, Ecol. Appl., 14, 72–88, https://doi.org/10.1890/01-6012, 2004.

Chambers, J. Q., Negron-Juarez, R. I., Marra, D. M., Di Vittorio, A., Tews, J., Roberts, D., Ribeiro, G. H. P. M., Trumbore, S. E., and Higuchi, N.: The steady-state mosaic of disturbance and succession across an old-growth Central Amazon forest landscape, P. Natl. Acad. Sci. USA, 110, 3949–3954, https://doi.org/10.1073/pnas.1202894110, 2013.

Chanca, I., Trumbore, S. E., Macario, K., and Sierra, C.: Probability distributions of radiocarbon in open linear compartmental systems at steady-state, J. Geophys. Res.-Biogeo., 127, e2021JG006673, https://doi.org/10.1029/2021JG006673, 2022.

Chanca, I., Levin, I., Trumbore, S., Macario, K., Lavric, J., Quesada, C. A., Araujo, A., Dias-Junior, C., van Asperen, H., Hammer, S., and Sierra, C.: Trace gases and isotope ratios (13C, 14C, 18O, 2H) of ambient air collected in flasks at a vertical profile at the ATTO site in October 2019, Max Planck Institute for Biogeochemistry [data set], https://doi.org/10.17871/atto.437.4.1683, 2024a.

Chanca, I., Levin, I., Trumbore, S., Macario, K., Lavric, J., Quesada, C. A., Araujo, A., Dias-Junior, C., van Asperen, H., Hammer, S., and Sierra, C.: Trace gases and isotope ratios (13C, 14C, 18O, 2H) of ambient air collected in flasks at a vertical profile at the ATTO site in December 2021, Max Planck Institute for Biogeochemistry [data set], https://doi.org/10.17871/ATTO.438.4.1684, 2024b.

de Araújo, A. C., Ometto, J. P. H. B., Dolman, A. J., Kruijt, B., Waterloo, M. J., and Ehleringer, J. R.: Implications of CO_2 pooling on $\delta^{13}C$ of ecosystem respiration and leaves in Amazonian forest, Biogeosciences, 5, 779–795, https://doi.org/10.5194/bg-5-779-2008, 2008.

Ehleringer, J. and Cook, C.: Carbon and oxygen isotope ratios of ecosystem respiration along an Oregon conifer transect: preliminary observations based on small-flask sampling, Tree Physiol., 18, 513–519, 1998.

Fung, I., Field, C. B., Berry, J. A., Thompson, M. V., Randerson, J. T., Malmström, C. M., Vitousek, P. M., Collatz, G. J., Sellers, P. J., Randall, D. A., Denning, A. S., Badeck, F., and John, J.: Carbon 13 exchanges between the atmosphere and biosphere, Global Biogeochem. Cy., 11, 507–533, https://doi.org/10.1029/97GB01751, 1997.

Gatti, L. V., Basso, L. S., Miller, J. B., Gloor, M., Gatti Domingues, L., Cassol, H. L. G., Tejada, G., Aragão, L. E. O. C., Nobre, C., Peters, W., Marani, L., Arai, E., Sanches, A. H., Corrêa, S. M., Anderson, L., Von Randow, C., Correia, C. S. C., Crispim, S. P., and Neves, R. A. L.: Amazonia as a carbon source linked to deforestation and climate change, Nature, 595, 388–393, https://doi.org/10.1038/s41586-021-03629-6, 2021.

Graven, H. D., Guilderson, T. P., and Keeling, R. F.: Observations of radiocarbon in CO_2 at seven global sampling sites in the Scripps flask network: Analysis of spatial gradients and seasonal cycles, J. Geophys. Res.-Atmos., 117, D02303, 2012.

Hammer, S. and Levin, I.: CORSO_14CO2_background_data_compilation, https://heibox.uni-heidelberg.de/d/1f481155f63c46a8aaf0/ (last access: 21 November 2023), 2023a.

Hammer, S. and Levin, I.: CORSO Deliverable 3.1 – Database of existing Δ14CO2 measurements, https://meta.icos-cp.eu/objects/HnpnYFcQljQ-SJer66F-hr-b (last access: 21 November 2023), 2023b.

Heimann, M., Jordan, A., Brand, W. A., Lavrič, J. V., Moossen, H., and Rothe, M.: The atmospheric flask sampling program of MPI-BGC, Version 13, 2022, Edmond – Open Research Data Repository of the Max Planck Society, https://doi.org/10.17617/3.8r, 2022.

Hua, Q., Turnbull, J. C., Santos, G. M., Rakowski, A. Z., Ancapichún, S., Pol-Holz, R. D., Hammer, S., Lehman, S. J., Levin, I., Miller, J. B., Palmer, J. G., and Turney, C. S. M.: Atmospheric radiocarbon for the period 1950–2019, Radiocarbon, 64, 723–745, https://doi.org/10.1017/RDC.2021.95, 2022.

Hubau, W., Lewis, S. L., Phillips, O. L., Affum-Baffoe, K., Beeckman, H., Cuní-Sanchez, A., Daniels, A. K., Ewango, C. E. N., Fauset, S., Mukinzi, J. M., Sheil, D., Sonké, B., Sullivan, M. J. P., Sunderland, T. C. H., Taedoumg, H., Thomas, S. C., White, L. J. T., Abernethy, K. A., Adu-Bredu, S., Amani, C. A., Baker, T. R., Banin, L. F., Baya, F., Begne, S. K., Bennett, A. C., Benedet, F., Bitariho, R., Bocko, Y. E., Boeckx, P., Boundja, P., Brienen,

R. J. W., Brncic, T., Chezeaux, E., Chuyong, G. B., Clark, C. J., Collins, M., Comiskey, J. A., Coomes, D. A., Dargie, G. C., de Haulleville, T., Kamdem, M. N. D., Doucet, J.-L., Esquivel-Muelbert, A., Feldpausch, T. R., Fofanah, A., Foli, E. G., Gilpin, M., Gloor, E., Gonmadje, C., Gourlet-Fleury, S., Hall, J. S., Hamilton, A. C., Harris, D. J., Hart, T. B., Hockemba, M. B. N., Hladik, A., Ifo, S. A., Jeffery, K. J., Jucker, T., Yakusu, E. K., Kearsley, E., Kenfack, D., Koch, A., Leal, M. E., Levesley, A., Lindsell, J. A., Lisingo, J., Lopez-Gonzalez, G., Lovett, J. C., Makana, J.-R., Malhi, Y., Marshall, A. R., Martin, J., Martin, E. H., Mbayu, F. M., Medjibe, V. P., Mihindou, V., Mitchard, E. T. A., Moore, S., Munishi, P. K. T., Bengone, N. N., Ojo, L., Ondo, F. E., Peh, K. S.-H., Pickavance, G. C., Poulsen, A. D., Poulsen, J. R., Qie, L., Reitsma, J., Rovero, F., Swaine, M. D., Talbot, J., Taplin, J., Taylor, D. M., Thomas, D. W., Toirambe, B., Mukendi, J. T., Tuagben, D., Umunay, P. M., van der Heijden, G. M. F., Verbeeck, H., Vleminckx, J., Willcock, S., Wöll, H., Woods, J. T., and Zemagho, L.: Asynchronous carbon sink saturation in African and Amazonian tropical forests, Nature, 579, 80–87, https://doi.org/10.1038/s41586-020-2035-0, 2020.

Jung, M., Schwalm, C., Migliavacca, M., Walther, S., Camps-Valls, G., Koirala, S., Anthoni, P., Besnard, S., Bodesheim, P., Carvalhais, N., Chevallier, F., Gans, F., Goll, D. S., Haverd, V., Köhler, P., Ichii, K., Jain, A. K., Liu, J., Lombardozzi, D., Nabel, J. E. M. S., Nelson, J. A., O'Sullivan, M., Pallandt, M., Papale, D., Peters, W., Pongratz, J., Rödenbeck, C., Sitch, S., Tramontana, G., Walker, A., Weber, U., and Reichstein, M.: Scaling carbon fluxes from eddy covariance sites to globe: synthesis and evaluation of the FLUXCOM approach, Biogeosciences, 17, 1343–1365, https://doi.org/10.5194/bg-17-1343-2020, 2020.

Keeling, C. D.: The concentration and isotopic abundances of atmospheric carbon dioxide in rural areas, Geochim. Cosmochim. Ac., 13, 322–334, https://doi.org/10.1016/0016-7037(58)90033-4, 1958.

Keeling, C. D.: The concentration and isotopic abundances of carbon dioxide in rural and marine air, Geochim. Cosmochim. Ac., 24, 277–298, https://doi.org/10.1016/0016-7037(61)90023-0, 1961.

Knohl, A., Werner, R. A., Brand, W. A., and Buchmann, N.: Short-term variations in $\delta^{13}C$ of ecosystem respiration reveals link between assimilation and respiration in a deciduous forest, Oecologia, 142, 70–82, 2005.

Kromer, B. and Münnich, K. O.: Co_2 Gas Proportional Counting in Radiocarbon Dating – Review and Perspective, in: Radiocarbon After Four Decades, edited by: Taylor, R. E., Long, A., and Kra, R. S., Springer, New York, NY, https://doi.org/10.1007/978-1-4757-4249-7_13, 1992.

Levin, I., Münnich, K., and Weiss, W.: The effect of anthropogenic CO_2 and ^{14}C sources on the distribution of ^{14}C in the atmosphere, Radiocarbon, 22, 379–391, https://doi.org/10.1017/S003382220000967X, 1980.

Levin, I., Naegler, T., Kromer, B., Diehl, M., Francey, R., Gomez-Pelaez, A., Steele, P., Wagenbach, D., Weller, R., and Worthy, D.: Observations and modelling of the global distribution and long-term trend of atmospheric $^{14}CO_2$, Tellus B, 62, 26–46, 2010.

Levin, I., Karstens, U., Eritt, M., Maier, F., Arnold, S., Rzesanke, D., Hammer, S., Ramonet, M., Vítková, G., Conil, S., Heliasz, M., Kubistin, D., and Lindauer, M.: A dedicated flask sampling strategy developed for Integrated Carbon Observation System (ICOS) stations based on CO_2 and CO measurements and Stochastic Time-Inverted Lagrangian Transport (STILT) footprint modelling, Atmos. Chem. Phys., 20, 11161–11180, https://doi.org/10.5194/acp-20-11161-2020, 2020.

Levin, I., Hammer, S., Kromer, B., Preunkert, S., Weller, R., and Worthy, D. E.: Radiocarbon in global tropospheric carbon dioxide, Radiocarbon, 64, 781–791, 2022.

Lu, X., Wang, Y.-P., Luo, Y., and Jiang, L.: Ecosystem carbon transit versus turnover times in response to climate warming and rising atmospheric CO_2 concentration, Biogeosciences, 15, 6559–6572, https://doi.org/10.5194/bg-15-6559-2018, 2018.

Lux, J. T.: A new target preparation facility for high precision AMS measurements and strategies for efficient $^{14}CO_2$ sampling, PhD thesis, Faculty of Physics and Astronomy/Institute of Environmental Physics, https://doi.org/10.11588/heidok.00024767, 2018.

Malhi, Y., Baldocchi, D., and Jarvis, P.: The carbon balance of tropical, temperate and boreal forests, Plant Cell Environ., 22, 715–740, https://doi.org/10.1046/j.1365-3040.1999.00453.x, 1999.

Malhi, Y., Doughty, C., and Galbraith, D.: The allocation of ecosystem net primary productivity in tropical forests, Philos. T. Roy. Soc. B, 366, 3225–3245, 2011.

Malhi, Y., Doughty, C. E., Goldsmith, G. R., Metcalfe, D. B., Girardin, C. A. J., Marthews, T. R., del Aguila-Pasquel, J., Aragão, L. E. O. C., Araujo-Murakami, A., Brando, P., da Costa, A. C. L., Silva-Espejo, J. E., Farfán Amézquita, F., Galbraith, D. R., Quesada, C. A., Rocha, W., Salinas-Revilla, N., Silvério, D., Meir, P., and Phillips, O. L.: The linkages between photosynthesis, productivity, growth and biomass in lowland Amazonian forests, Global Change Biol., 21, 2283–2295, https://doi.org/10.1111/gcb.12859, 2015.

Marsh, E. J., Bruno, M. C., Fritz, S. C., Baker, P., Capriles, J. M., and Hastorf, C. A.: IntCal, SHCal, or a mixed curve? Choosing a ^{14}C calibration curve for archaeological and paleoenvironmental records from tropical South America, Radiocarbon, 60, 925–940, 2018.

Mauritz, M., Celis, G., Ebert, C., Hutchings, J., Ledman, J., Natali, S. M., Pegoraro, E., Salmon, V. G., Schädel, C., Taylor, M., and Schuur, E. A. G.: Using Stable Carbon Isotopes of Seasonal Ecosystem Respiration to Determine Permafrost Carbon Loss, J. Geophys. Res.-Biogeo., 124, 46–60, https://doi.org/10.1029/2018JG004619, 2019.

Metzler, H. and Sierra, C. A.: Linear autonomous compartmental models as continuous-time Markov chains: Transit-time and age distributions, Math. Geosci., 50, 1–34, https://doi.org/10.1007/s11004-017-9690-1, 2018.

Miller, J. B. and Tans, P. P.: Calculating isotopic fractionation from atmospheric measurements at various scales, Tellus B, 55, 207–214, https://doi.org/10.3402/tellusb.v55i2.16697, 2003.

Miller, J. B., Lehman, S. J., Verhulst, K. R., Miller, C. E., Duren, R. M., Yadav, V., Newman, S., and Sloop, C. D.: Large and seasonally varying biospheric CO_2 fluxes in the Los Angeles megacity revealed by atmospheric radiocarbon, P. Natl. Acad. Sci. USA, 117, 26681–26687, 2020.

Muñoz, E., Chanca, I., and Sierra, C. A.: Increased atmospheric CO_2 and the transit time of carbon in terrestrial ecosystems, Glob. Change Biol., 29, 6441–6452, https://doi.org/10.1111/gcb.16961, 2023.

Ometto, J. P., Flanagan, L. B., Martinelli, L. A., Moreira, M. Z., Higuchi, N., and Ehleringer, J. R.: Carbon isotope discrimination in forest and pasture ecosystems of the Amazon Basin, Brazil, Global Biogeochem. Cy., 16, 56-1–56-10, 2002.

Pataki, D., Ehleringer, J., Flanagan, L., Yakir, D., Bowling, D., Still, C., Buchmann, N., Kaplan, J. O., and Berry, J.: The application and interpretation of Keeling plots in terrestrial carbon cycle research, Global Biogeochem. Cy., 17, 1022, https://doi.org/10.1029/2001GB001850, 2003.

Phillips, C. L., McFarlane, K. J., LaFranchi, B., Desai, A. R., Miller, J. B., and Lehman, S. J.: Observations of $^{14}CO_2$ in ecosystem respiration from a temperate deciduous forest in Northern Wisconsin, J. Geophys. Res.-Biogeo., 120, 600–616, https://doi.org/10.1002/2014JG002808, 2015.

Phillips, O. L. and Brienen, R. J.: Carbon uptake by mature Amazon forests has mitigated Amazon nations' carbon emissions, Carbon Balance and Management, 12, 1–9, 2017.

Pöhlker, C., Walter, D., Paulsen, H., Könemann, T., Rodríguez-Caballero, E., Moran-Zuloaga, D., Brito, J., Carbone, S., Degrendele, C., Després, V. R., Ditas, F., Holanda, B. A., Kaiser, J. W., Lammel, G., Lavrič, J. V., Ming, J., Pickersgill, D., Pöhlker, M. L., Praß, M., Löbs, N., Saturno, J., Sörgel, M., Wang, Q., Weber, B., Wolff, S., Artaxo, P., Pöschl, U., and Andreae, M. O.: Land cover and its transformation in the backward trajectory footprint region of the Amazon Tall Tower Observatory, Atmos. Chem. Phys., 19, 8425–8470, https://doi.org/10.5194/acp-19-8425-2019, 2019.

Rasmussen, M., Hastings, A., Smith, M. J., Agusto, F. B., Chen-Charpentier, B. M., Hoffman, F. M., Jiang, J., Todd-Brown, K. E. O., Wang, Y., Wang, Y.-P., and Luo, Y.: Transit times and mean ages for nonautonomous and autonomous compartmental systems, J. Math. Biol., 73, 1379–1398, https://doi.org/10.1007/s00285-016-0990-8, 2016.

Reimer, P. J., Brown, T. A., and Reimer, R. W.: Discussion: reporting and calibration of post-bomb ^{14}C data, Radiocarbon, 46, 1299–1304, 2004.

Saturno, J., Holanda, B. A., Pöhlker, C., Ditas, F., Wang, Q., Moran-Zuloaga, D., Brito, J., Carbone, S., Cheng, Y., Chi, X., Ditas, J., Hoffmann, T., Hrabe de Angelis, I., Könemann, T., Lavrič, J. V., Ma, N., Ming, J., Paulsen, H., Pöhlker, M. L., Rizzo, L. V., Schlag, P., Su, H., Walter, D., Wolff, S., Zhang, Y., Artaxo, P., Pöschl, U., and Andreae, M. O.: Black and brown carbon over central Amazonia: long-term aerosol measurements at the ATTO site, Atmos. Chem. Phys., 18, 12817–12843, https://doi.org/10.5194/acp-18-12817-2018, 2018.

Sedjo, R. and Sohngen, B.: Carbon sequestration in forests and soils, Annu. Rev. Resour. Econ., 4, 127–144, 2012.

Sierra, C. A., Harmon, M. E., Moreno, F. H., Orrego, S. A., and del Valle, J. I.: Spatial and temporal variability of net ecosystem production in a tropical forest: testing the hypothesis of a significant carbon sink, Global Change Biol., 13, 838–853, https://doi.org/10.1111/j.1365-2486.2007.01336.x, 2007.

Sierra, C. A., Müller, M., Metzler, H., Manzoni, S., and Trumbore, S. E.: The muddle of ages, turnover, transit, and residence times in the carbon cycle, Global Change Biol., 23, 1763–1773, https://doi.org/10.1111/gcb.13556, 2017.

Sierra, C. A., Crow, S. E., Heimann, M., Metzler, H., and Schulze, E.-D.: The climate benefit of carbon sequestration, Biogeosciences, 18, 1029–1048, https://doi.org/10.5194/bg-18-1029-2021, 2021a.

Sierra, C. A., Estupinan-Suarez, L. M., and Chanca, I.: The fate and transit time of carbon in a tropical forest, J. Ecol., 109, 2845–2855, https://doi.org/10.1111/1365-2745.13723, 2021b.

Sierra, C. A., Quetin, G. R., Metzler, H., and Müller, M.: A decrease in the age of respired carbon from the terrestrial biosphere and increase in the asymmetry of its distribution, Philos. T. Roy. Soc. A, 381, 20220200, https://doi.org/10.1098/rsta.2022.0200, 2023.

Stephens, B. B., Gurney, K. R., Tans, P. P., Sweeney, C., Peters, W., Bruhwiler, L., Ciais, P., Ramonet, M., Bousquet, P., Nakazawa, T., Aoki, S., Machida, T., Inoue, G., Vinnichenko, N., Lloyd, J., Jordan, A., Heimann, M., Shibistova, O., Langenfelds, R. L., Steele, L. P., Francey, R. J., and Denning, A. S.: Weak Northern and Strong Tropical Land Carbon Uptake from Vertical Profiles of Atmospheric CO_2, Science, 316, 1732–1735, https://doi.org/10.1126/science.1137004, 2007.

Steur, P. M., Botter, D., Scheeren, H. A., Moossen, H., Rothe, M., and Meijer, H. A.: Preventing drift of oxygen isotopes of CO_2-in-air stored in glass sample flasks: new insights and recommendations, Isot. Environ. Healt. S., 59, 309–326, 2023.

Stuiver, M. and Polach, H. A.: Discussion reporting of ^{14}C data, Radiocarbon, 19, 355–363, https://doi.org/10.1017/S0033822200003672, 1977.

Tans, P. P.: On calculating the transfer of carbon-13 in reservoir models of the carbon cycle, Tellus, 32, 464–469, 1980.

Telles, E. d. C. C., de Camargo, P. B., Martinelli, L. A., Trumbore, S. E., da Costa, E. S., Santos, J., Higuchi, N., and Oliveira Jr., R. C.: Influence of soil texture on carbon dynamics and storage potential in tropical forest soils of Amazonia, Global Biogeochem. Cy., 17, 1040, https://doi.org/10.1029/2002GB001953, 2003.

Thoning, K. W., Tans, P. P., and Komhyr, W. D.: Atmospheric carbon dioxide at mauna loa observatory: 2. Analysis of the NOAA GMCC data, 1974–1985, J. Geophys. Res.-Atmos., 94, 8549–8565, 1989.

Trumbore, S.: Carbon respired by terrestrial ecosystems – recent progress and challenges, Global Change Biol., 12, 141–153, https://doi.org/10.1111/j.1365-2486.2006.01067.x, 2006.

Trumbore, S. and De Camargo, P. B.: Soil carbon dynamics, Amazonia and Global Change, 186, 451–462, https://doi.org/10.1029/2008GM000741, 2009.

Trumbore, S., Da Costa, E. S., Nepstad, D. C., Barbosa De Camargo, P., Martinelli, L. A., Ray, D., Restom, T., and Silver, W.: Dynamics of fine root carbon in Amazonian tropical ecosystems and the contribution of roots to soil respiration, Global Change Biol., 12, 217–229, https://doi.org/10.1111/j.1365-2486.2005.001063.x, 2006.

Turnbull, J. C., Mikaloff Fletcher, S. E., Ansell, I., Brailsford, G. W., Moss, R. C., Norris, M. W., and Steinkamp, K.: Sixty years of radiocarbon dioxide measurements at Wellington, New Zealand: 1954–2014, Atmos. Chem. Phys., 17, 14771–14784, https://doi.org/10.5194/acp-17-14771-2017, 2017.

Vieira, S., Trumbore, S., Camargo, P. B., Selhorst, D., Chambers, J. Q., Higuchi, N., and Martinelli, L. A.: Slow growth rates of Amazonian trees: consequences for carbon cycling, P. Natl. Acad. Sci. USA, 102, 18502–18507, https://doi.org/10.1073/pnas.0505966102, 2005.

Wendeberg, M., Richter, J. M., Rothe, M., and Brand, W. A.: Jena Reference Air Set (JRAS): a multi-point scale anchor for isotope measurements of CO_2 in air, Atmos. Meas. Tech., 6, 817–822, https://doi.org/10.5194/amt-6-817-2013, 2013.

Zobitz, J., Keener, J., Schnyder, H., and Bowling, D.: Sensitivity analysis and quantification of uncertainty for isotopic mixing relationships in carbon cycle research, Agr. Forest Meteorol., 136, 56–75, 2006.